Molecular Mobility in Supercooled Trehalose

A. De Gusseme, L. Carpentier,* J. F. Willart, and M. Descamps

Laboratoire de Dynamique et Structure des Matériaux Moléculaires, UMR 8024, Bât. P5, Université des Sciences et Technologies de Lille, 59655 Villeneuve d'Ascq Cedex, France

Received: February 7, 2003; In Final Form: June 27, 2003

The molecular mobility of amorphous anhydrous trehalose ($C_{12}H_{22}O_{11}$) was investigated by means of temperature-modulated differential scanning calorimetry (TMDSC) and dielectric analysis (DEA). TMDSC was used to perform a specific heat spectroscopy, which appeared essential, as dielectric measurements above T_g were hampered by dc conductivity. TMDSC and DEA are useful complementary techniques for the study of the molecular mobility of this important bioprotecting agent. The study of the primary relaxation of trehalose, above the glass transition temperature, yielded the determination of the fragility index *m* and the stretching exponent β. The correlation between *m* and β was also discussed. Dielectric studies of the sub-T_g domain highlighted two distinct secondary relaxation processes, whose dynamical features were evaluated.

1. Introduction

α,α-Trehalose (α-D-glucopyranosyl, **α**-D-glucopyranoside), is a nonreducing disaccharide of glucose. It commonly exists as a dihydrate,[1,2] and transforms upon heating into a stable anhydrous T_β form.[3] In this dehydration process, a transient, history-dependent metastable form of yet unknown structure, T_α, has also been found.[4−6] Trehalose is widely found in various "anhydrobiotic" organisms (such as yeast, fungi, mushroom, scorpions, and more generally the animal and vegetal life of desert regions) that are able to survive almost complete dehydration. Actually, bioprotective skills are a common feature to many carbohydrates.[7] Among other disaccharides, trehalose appears exceptionally efficient in stabilizing labile molecules,[8,9] and numerous studies have been motivated by this property.

Despite these various investigations, the origin of the exceptional bioprotective skills of trehalose remains controversial. The specificity of the glassy character of trehalose has been invoked to explain the efficiency of this sugar in preserving life.[10] Trehalose has the highest glass transition temperature T_g of the disaccharides.[11] Moreover, the binary systems trehalose/water exhibit glass transition temperatures that are noticeably higher than those of other disaccharide/water systems, at identical concentration.[12] Their fragile character has also been underlined.[13] Ding et al.[14] suggested that the specific evolution of the T_g of the trehalose/water system, as a function of the sugar content, allowed dynamic processes to be slowed by vitrification at temperatures as high as ambient. This would ensure that life is suspended while maintaining relatively high water content, thus limiting cell damage.

However, we wonder if the intrinsic properties of the vitreous state itself constitute a crucial element that plays a key role in the bioprotective action of trehalose. The formation of layers of glassy anhydrous trehalose, coating labile molecules, has already been invoked as a possible biopreservation mechanism.[15] Undoubtedly, better knowledge of the temperature dependence of the relaxation times $\tau(T)$ in trehalose should contribute to the understanding of the exceptional properties of this sugar.

* To whom correspondence should be addressed: Laurent.Carpentier@univ-lille1.fr.

Above T_g, the dependence is usually described by a Vogel−Fulcher−Tammann (VFT) equation:

$$\tau(T) = \tau_0 \exp\left(\frac{DT_0}{T - T_0}\right) \quad (1)$$

This equation simplifies to the Arrhenius law when T_0 becomes 0. Glass-forming systems are most commonly classified according to their fragility. The fragility can be quantified by the steepness index "*m*", that is, the slope at T_g of the VFT curve in a T_g-scaled Arrhenius plot.[16] A system is said to be all the more fragile as the value of *m* is high, i.e., as the degree of departure from the Arrhenius behavior is large. Sub-T_g mobility, particularly the so-called β Johari-Goldstein relaxation,[17] is also of considerable interest. It raises numerous fundamental problems, as its origin remains poorly understood.[18] It is suspected to be a universal feature of the glass dynamics and to be responsible for unusual sub-T_g nucleation processes.[19] Moreover, it constitutes a crucial issue from the point of view of biopreservation, since this residual mobility is believed to be instrumental in achieving stability.

Surprisingly, information on the molecular mobility in dry amorphous trehalose is relatively scarce in the literature. Until now, most studies have focused on the thermodynamic properties of the trehalose/water system.[12,13,20] Magazu et al.[12] and Elias et al.[13] have performed viscosity measurements on the mixture trehalose/water. Their respective investigations both revealed the fragile character of the trehalose/water system but inferred significantly different values of the fragility index m for the same concentration range ($m = 120$[12] or $m = 165$[13] for a sugar mass concentration of 0.5). On the other hand, few publications have dealt with the dynamical features of pure trehalose. In a recent paper,[15] Sussich and co-workers mentioned values of *m* for trehalose ranging from 60 to 180. This latter result is rather surprising, because to the best of our knowledge, such high values of the fragility index have only been reported for polymers of much higher molecular weights.[21] Shamblin et al.[22,23] performed differential scanning calorimetry (DSC) experiments to evaluate relaxation times in trehalose and other pharmaceutical glasses. They aimed at predicting the temper-

10.1021/jp0343234 CCC: $25.00
Published on Web 09/09/2003

atures where the relaxation times of such glasses exceeded practical storage times; however, their approach did not include the evaluation of the fragility index.

In this paper, we present the outcomes of investigations of the molecular mobility in dry amorphous trehalose, above and below T_g. These results were obtained by the combined use of two techniques: dielectric spectroscopy and temperature-modulated differential scanning calorimetry (TMDSC). The latter allowed us to perform a specific heat spectroscopy, by probing the evolution of the enthalpic relaxation modes that freeze at the calorimetric T_g. It was used advantageously because our low-frequency dielectric measurements were hampered by conductivity. Section 2 briefly presents one possible way to analyze the TMDSC signals for the purpose of specific heat spectroscopy. Details of this technique can be found in refs 24−27. Experimental details are given in section 3. Section 4 gathers together the results of TMDSC and dielectric experiments performed on trehalose, above T_g. Section 5 presents a dielectric study of the sub-T_g molecular mobility in glassy trehalose. These results are collectively discussed in section 6.

2. TMDSC as a Specific Heat Spectroscopy Technique

The principles of the TMDSC technique have been described in several papers.[24,25] In this section, we briefly summarize a possible exploitation of the TMDSC signals, in terms of specific heat spectroscopy. Additional details are available from refs 26 and 27.

2.1. Oscillating Perturbation and Response. TMDSC is a scanning technique in which a small sinusoidal temperature change is added to the conventional DSC temperature ramp $\bar{T}(t)$:

$$T(t) = \bar{T}(t) + T_{sm} = T_i + qt + A \sin \omega t \qquad (2)$$

where T_i is the initial temperature, q the underlying scanning rate, and A the amplitude of the sinusoidal modulation. The accessible pulsations ω range between 0.063 and 0.63 Hz. It is appropriate to consider the modulated temperature rate as the perturbation:

$$\dot{T}(t) = q + \dot{T}_0 \cos \omega t; \quad \dot{T}_0 = A\omega \qquad (3)$$

The resultant heat flow involves a linear part and an out of phase sinusoidal modulated part $\dot{Q}_{sin}(t)$, to which may be added a kinetic contribution $\dot{Q}_{kin}$ (induced by kinetic effects such as cold crystallization or enthalpy recovery observed upon heating an annealed glass) that we will not consider here:

$$\dot{Q}(t) = qC_p(q,\bar{T}) + (\dot{Q}_{kin}) + \dot{Q}_0(\bar{T},\omega) \cos(\omega t - \varphi) \qquad (4)$$

$$\dot{Q}_{sin}(t) = \dot{Q}_0(\bar{T},\omega) \cos(\omega t - \varphi) \qquad (5)$$

In expression (4), the first two terms are those of a conventional DSC experiment. $C_p(q,\bar{T})$ is the heat capacity of the sample, as measured by this technique.

Figure 1a shows typical TMDSC signals obtained upon heating amorphous trehalose at 1 K/min. Amorphous trehalose was obtained by cooling the liquid to ambient temperature, at 1 K/min. The characteristic features of the approach of the glass transition shown by this TMDSC measurement are

(a) the classical jump of the average heat flow $\langle \dot{Q}(t) \rangle$ at $T_g^{1K/min} = 396$ K,

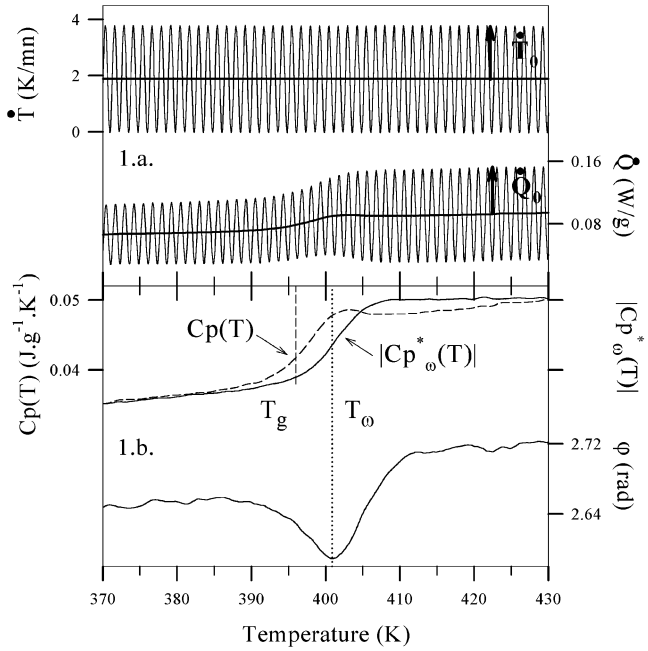

Figure 1. (a) Evolution of the main TMDSC signals (modulated temperature $\dot{T}(t)$ and the modulated heat flow $\dot{Q}(t)$) for quenched trehalose, upon heating. Experimental parameters are underlying heating rate $q = 1$ K/min, modulation period $\omega/2\pi = 10^{-2}$ s, and modulation amplitude $A = 0.053$ K. (b) Complex heat capacity $C_p^*(\omega)$ of quenched trehalose, calculated from $\dot{T}(t)$ and $\dot{Q}(t)$. The phase lag φ exhibits a peak at T_ω, whose maximum arises with a jump in $|C_p^*(\omega|$. This temperature T_ω is higher than the calorimetric glass transition temperature $T_g^{q=1K/\ min}$.

(b) the jump of the modulated heat flow amplitude $\dot{Q}_0$ at a temperature somewhat higher, $T_\omega = 401$ K,

and (c) a peak in the phase lag φ at T_ω.

The glass transition temperature observed upon heating strongly depends on the rate at which the liquid was quenched. For liquid trehalose cooled at 1 K/min, the glass transition upon reheating with the same scanning rate occurs at $T_{g\,(q)}^{1K/min} = 396$ K. T_ω reveals a different ergodicity breaking temperature associated with the shorter time scale of the oscillating perturbation.

2.2. Phase Correction. The phase lag φ displayed on Figure 1b is nonzero over the whole temperature range. It actually includes two contributions: one of purely relaxational origin and one that has been attributed to heat transfers, both between the sample and the calorimeter and within the sample itself.[28,29] In a specific heat spectroscopy analysis, only the relaxational part φ_0 and its temperature and frequency dependence should be taken into account. The phase lag φ thus needs to be corrected, to remove the contribution due to heat transfers. Weyer et al.[29] have proposed to perform this correction by subtracting a curve which is proportional to the measured heat capacity and scaled in such a way that it fits to the measured phase angle outside the glass transition region.

2.3. Complex Heat Capacity. With a complex notation, the modulated heat flow is related to the complex heat capacity $C_p^*(\omega)$ by the expression:

$$\dot{Q}_{sin}(t) = \text{Real}(\dot{Q}_{sin}^* e^{-i\omega t}) = \text{Real}(C_p^*(\omega) T_0 e^{-i\omega t}) \qquad (6)$$

The real and imaginary parts of $C_p^*(\omega)$ are thus given by

$$C' = \frac{\dot{Q}_0}{\dot{T}_0} \cos \varphi_0 \qquad (7)$$

and

$$C'' = \frac{\dot{Q}_0}{\dot{T}_0}\sin\varphi_0 \tag{8}$$

$C_p^*(\omega)$ can be determined in the course of a routine TMDSC scan. As was previously discussed,[25] the signal can be displaced and distorted to give an effective "leveling" when the two characteristic times of the technique, respectively related to the scanning rate and the modulation, are close. This drawback can be largely avoided by using low values for q.

3. Experimental Section

3.1 Trehalose. Crystalline trehalose dihydrate ($C_{12}H_{22}O_{11}$·$2H_2O$) was purchased from Fluka, with a guaranteed purity of more than 99%. It was used without further purification. The sugar molecule is constituted of two glucopyranose rings, as illustrated below:

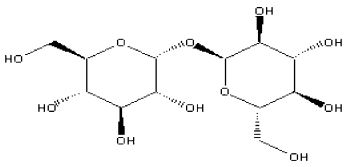

Trehalose : $C_{12}H_{22}O_{11}$

3.2. Temperature-Modulated Differential Scanning Calorimetry. Calorimetric experiments were carried out in a TA Instruments DSC 2920, equipped with a refrigerated cooling system. The trehalose samples were encapsulated in aluminum open pans, so as not to hinder dehydration upon heating. The samples mass was about 5 mg, which is a low enough value to allow the samples to follow the imposed thermal oscillations. Amorphous trehalose was prepared directly in the DSC oven: once molten ($T_m = 483$ K), trehalose can be easily undercooled at 1 K/min. When reheated at the same scanning rate, it undergoes a glass transition at $T_g^{1K/min} = 396$ K (Figure 1). During the experiments, the trehalose samples, which are prone to hydration, were kept under a constant helium flow, so as to preserve them from ambient humidity and to ensure reproducible experiments. The experimental baseline was calibrated by scanning the whole temperature domain with an empty pan, using the same scanning rate as in the experiments. Temperature and enthalpy calibrations were performed with indium as a standard. For the specific heat spectroscopy experiments, we have used an extremely slow scanning rate ($q = -0.1$ K/min), which ensures the separation of the two characteristic times of the technique, respectively related to the scanning rate and the modulation frequency (cf. section 2). The modulus of the complex heat capacity was calibrated from the C_p measurements of sapphire in the studied temperature range.

3.3. Dielectric Analysis. Dielectric measurements were performed with a TA Instruments dielectric analyzer DEA 2970, which supplied more than 7 decades of frequencies (1 mHz−3 × 10^5 Hz), thus facilitating a complete assessment of the glass behavior. A liquid nitrogen cooling accessory provided testing capability from 130 to 700 K. The dielectric cell consists of an interdigitated array of electrodes on which the samples were molten, to ensure an optimal filling of the cell. During each experiment, the trehalose samples were maintained under a dry nitrogen gas flow, which prevented them from adsorbing ambient humidity. In the sub-T_g domain, the samples were subjected to a constant compressive force, which guaranteed good contacts between the sample and the sensor. The complex dielectric susceptibility was measured by both temperature ramps (heating rate 1 K/min) and isothermal scans. The isochronal measurements gave a general overview of the different relaxation processes, whereas the isothermal scans yielded a more precise description of the relaxations.

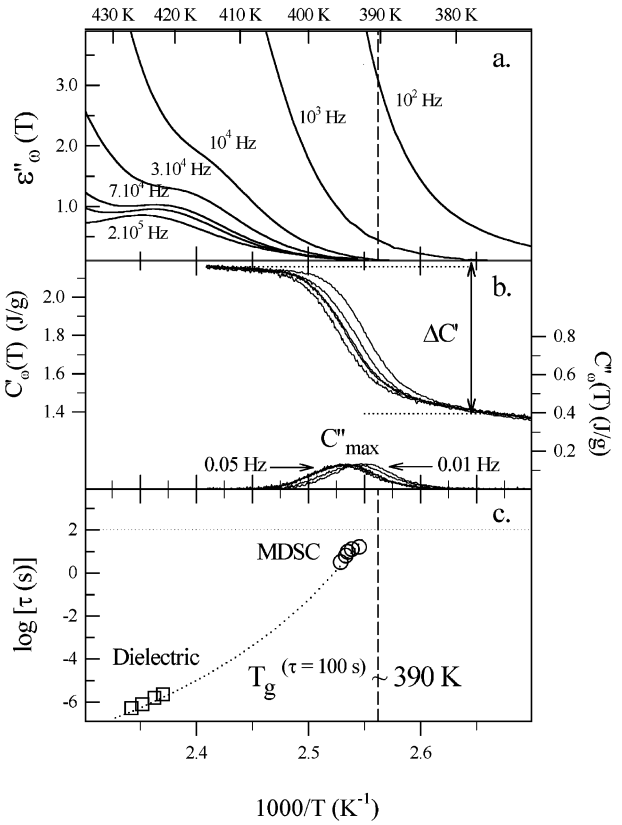

Figure 2. (a) Dielectric loss $\epsilon''_\omega(T)$ of quenched trehalose, recorded upon heating at 1 K/min and plotted as a function of inverse temperature. The peaks detectable at high frequencies correspond to the primary relaxation process α. At low frequencies, the measurement is hampered by ionic conductivity. (b) Real and imaginary parts of the complex specific heat $C_p^*(\omega)$, recorded upon cooling the sample at 0.1 K/min and plotted versus reciprocal temperature. The investigated modulation periods range from 20 to 100 s, by steps of 20 s. (c) Arrhenius diagram for trehalose, showing the evolution of the characteristic relaxation time τ as a function of inverse temperature. The dotted line is a guide for the eye.

4. Primary Relaxations

The primary relaxations are those involved in the dramatic slowing down of the dynamics on approaching the glass transition temperature, which eventually leads to structural arrest at T_g on the laboratory time scale.[30] They were investigated here by means of dielectric and specific heat spectroscopy.

4.1 Dielectric Measurements. Figure 2a shows the results of dielectric isochronal measurements performed on a sample of quenched trehalose. The imaginary part of the complex dielectric susceptibility, $\epsilon''_\omega(T)$, is plotted versus inverse temperature. Data were recorded upon cooling the sample from 453 to 333 K, at 1 K/min, while scanning a frequency domain covering more than 5 decades (1 Hz to 2 × 10^5 Hz).

Only the curves corresponding to the highest investigated frequencies (i.e., 2 × 10^5, 10^5, and 70 000 Hz) display a well-defined relaxation peak corresponding to the α process. As the frequency is raised, the peak becomes better resolved, and its

maximum shifts toward high temperatures (T_{max} = 422 K at 70 000 Hz and 425 K at 2×10^5 Hz). This shift is relatively small, thus suggesting that the activation energy for the α process in trehalose is important.

At lower frequencies, the dc contribution to the dielectric response becomes so important that a reliable measurement of $\epsilon''_\omega(T)$ is no longer possible. At 30 000 and 10 000 Hz the α relaxation process becomes only perceivable through a slight shoulder on the conductivity curve, which makes the localization of the maximum difficult. At frequencies lower than 10^4 Hz, the dielectric curves are absolutely featureless. Moreover, such an important ionic conductivity contribution prevents isothermal measurements. To compensate the lack of data in the low-frequency domain, TMDSC was used as a specific heat spectroscopy technique (cf. section 2).

4.2. Temperature-Modulated DSC Measurements. The TMDSC technique offers the possibility to explore a frequency domain ranging from 0.01 to 0.1 Hz. It therefore probes the enthalpic relaxation modes, which are also those observed in a conventional DSC scan.

TMDSC data were acquired upon repeated temperature scans at 0.1 K/min, from 408 to 368 K. It has been shown that, for such a low cooling rate, the data are reversible.[25] The measured $C_p^*(T)$ thus corresponds to the heat capacity of the equilibrium metastable liquid. Performing the measurements upon cooling allowed the enthalpy recovery effect to be avoided, characteristic of annealed glasses. The investigated modulation periods ($P = 2\pi/\omega$) varied from 20 to 100 s, by steps of 20 s. The modulation amplitudes A were chosen so that the perturbation amplitude remained constant in all the experiments: $\dot{T}_0 = A\omega = \pi/100$ K s^{-1}.

Data presented in Figure 2b were analyzed in terms of complex components of $C_p^*(T)$ by using the equations of section 2. Figure 2b shows the real and imaginary parts of the complex specific heat of liquid trehalose, as a function of inverse temperature, for each investigated frequency. The $C''_\omega(T)$ curves display peaks, whose maxima arise at the same temperature T_ω where the real part $C'_\omega(T)$ drops. The $C'_\omega(T)$ and $C''_\omega(T)$ curves therefore exhibit the characteristic behavior of the complex susceptibility of a relaxation process. The temperature T_ω of the enthalpy loss maximum increases with ω. It corresponds to the temperature where the characteristic relaxation time of the sample $\tau(T_\omega) = 1/\omega$ is the most probable. The curves' evolution indicates that the relaxation times in the liquid increase as T is lowered. Spectroscopic information about the activation energy and the (non)exponentiality of the relaxations can be deduced from these measurements.

4.3. Activation Energy and Fragility. The Arrhenius plot presented on Figure 2c gathers together the spectroscopic information obtained both by specific heat and dielectric spectroscopy, performed above the glass transition temperature. The figure emphasizes the coherence of the global evolution of the relaxation times measured by both techniques. Our results thus demonstrate that the relaxation modes involved in the dielectric relaxation of pure trehalose contribute significantly to those involved in the enthalpic relaxation.

Moreover, they illustrate the usefulness of TMDSC to obtain dynamic information near T_g, especially when dielectric measurements are difficult due to dc conductivity. Even so, the scarcity of the dielectric data above T_g prevented us from fitting the temperature dependence of the primary relaxations with the usual Vogel-Fulcher-Tamman expression.[30] We focus in this section on the dynamical information that could be obtained from the sole TMDSC results.

As could be expected over such a narrow frequency domain, TMDSC data exhibit Arrhenius behavior:

$$\tau(T_\omega) = \tau_0 \exp\left(\frac{E}{RT_\omega}\right) \tag{9}$$

In this expression, the prefactor τ_0 is the characteristic relaxation time at infinite temperature and E is the activation energy. A fit of our experimental results to the above Arrhenius law yields E = 800 kJ/mol and $\tau_0 = 10^{-105}$ s. These values obviously have no direct physical meaning but indicate that the general temperature dependence of the relaxation times of the system must be strongly non-Arrhenius.

TMDSC data, close to T_g, are especially convenient for the determination of the fragility index of a glass-forming system, which is a way to assess its non-Arrhenius behavior.[16] In a T_g-scaled Arrhenius plot, the fragility index m measures how fast τ changes with T_g/T at the glass temperature T_g, and it is thus given by

$$m = \left|\frac{\mathrm{d}(\log \tau)}{\mathrm{d}(T_g/T)}\right|_{T=T_g} = \frac{E}{RT_g(\tau = 100 \text{ s}) \ln 10} \tag{10}$$

The glass transition temperature T_g, at which the relaxation time is 100 s, was deduced from the TMDSC experiments to be equal to **390 K**. This result is consistent with the calorimetric T_g, which attests to the reliability of the relaxation times measured by this technique. The determination of T_g enabled us to calculate m for trehalose using eq 10, from which we obtain $m^{\text{trehalose}} = \mathbf{107}$. The estimated error on the m value is directly linked to the standard deviation of the linear regression used to calculate the activation energy E. This error is estimated to ±20 kJ/mol for E, which corresponds to a ±3 error for the m value. The high value of m reflects the fragile character of trehalose, which correlates well with the apparent strong deviation from Arrhenius behavior suggested by the TMDSC results.

4.4. Nonexponentiality. Additional information on the dynamics of the glass-forming system is also provided by the evaluation of its nonexponential behavior. Relaxations of glass formers are usually nonexponential, and it has been shown that this tendency is all the more pronounced as the glass former is more fragile.[31] The description of the nonexponential character is often made by using the fractional exponent β_{KWW} of the Kolrausch-Williams-Watt (KWW) relaxation function of any investigated quantity:[32]

$$\Phi(t) = \exp\left[-\left(\frac{t}{\tau}\right)^{\beta_{KWW}}\right] \tag{11}$$

When investigations are performed in the frequency domain, the value of β_{KWW} is related to the width of the relaxation peak, β_{KWW} being all the smaller as the width of the peak exceeds the 1.14 decades predicted for a pure Debye relaxation. This stretched exponential behavior is believed to reflect the intermolecular coupling.[33] The intermolecular coupling in addition to the Adam-Gibbs theory are invoked to give rise to the non-Arrhenius VFT dependence of the relaxation times.

No reliable data about the nonexponential evolution of the features of the relaxation function in trehalose could be obtained from the dielectric measurements. However, the stretching exponent β_{KWW} could be estimated from the isochronal specific heat spectroscopy data, according to the method proposed by Böhmer et al.[34] This method utilizes the amplitudes of the real and imaginary parts of the susceptibility: χ'_ω and χ''_ω. In the case of an exponential Debye relaxation function ($\beta_{KWW} = 1$),

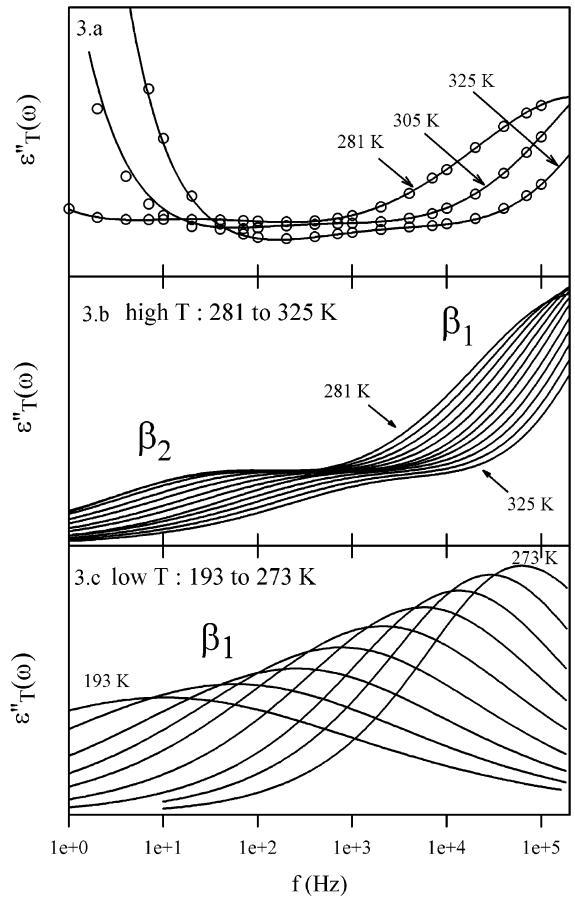

Figure 3. (a) Evolution of the dielectric loss $\epsilon''_T(\omega)$ of supercooled trehalose, recorded during isothermal scans at 281, 305, and 325 K. Open circles, experimental points; solid lines, fitted curves. The low-frequency wing of the spectra is the dc conductivity contribution. (b) "High-temperature" (281−325 K) evolution of the fitted $\epsilon''_T(\omega)$ curves of supercooled trehalose, from which the conductivity contribution was subtracted. The curves evidence two distinct secondary relaxation processes, respectively denoted β_1 (high-frequency process) and β_2 (low-frequency process). (c) "Low-temperature" (193−273 K) continuation of the β_1 process, which was separated from the main figure for clarity.

the magnitude of the loss peak χ''_{max} normalized by the dispersion step, $\Delta\chi' = \chi'_{\omega=0} - \chi'_{\omega=\infty}$, is 0.5. The ratio $\chi''_{max}/\Delta\chi'$ becomes smaller when β_{KWW} decreases, with increasing departure from exponential decay. This correlation has been tabulated by Moynihan and al.[35] by evaluation of the Fourier transform of the derivative of the decay (KWW) function and shown to provide accurate values of β_{KWW}. We applied this argument to the above TMDSC results, to determine the nonexponentiality of trehalose from the $C'(T)$ and $C''(T)$ curves. The marked nonexponential behavior of the primary relaxations of trehalose is demonstrated by the low value of $\beta_{KWW,treh} = 0.30$.

5. Sub-T_g Relaxations

Dielectric experiments in the sub-T_g domain highlighted an important secondary relaxation in glassy trehalose. We reported on Figure 3 the imaginary part of the dielectric susceptibility, that reveals the essential features of this so-called β relaxation.

Figure 3.a displays the isothermal dielectric loss curves of supercooled anhydrous trehalose, plotted against the frequency on a logarithmic scale, for three different temperatures: 281, 305, and 325 K (open circles). The overall aspect of the sub-T_g dielectric spectra of quenched trehalose reveals an important residual molecular mobility. In fact, two relaxation processes can be distinguished on Figure 3a:

a prominent "β_1 process" at high frequency that is visible at 281 K but shifts out of the available frequency window at higher temperatures and

another "β_2 process" of much smaller amplitude, occurring at lower frequency (10^2−10^4 Hz at 325 K).

In addition to these two processes, an important dc conductivity contribution prevents accurate observation of the dielectric signal at low frequency, especially at temperatures above 305 K. Experimental results were therefore fitted with a combination of two Cole−Cole functions, to which a conductivity term σ_{dc} was added:

$$\epsilon^*(\omega) = \sum_{i=1}^{2}\left(\epsilon_{\infty i} + \frac{\epsilon_{si} - \epsilon_{\infty i}}{1 + (i\omega\tau_i)^{\alpha}i}\right) + \sigma_{dc} \qquad (12)$$

The dielectric constants in the limits of high and low frequency are respectively denoted ϵ_∞ and ϵ_s, and τ_i sets the characteristic time scale of the corresponding process. The temperature-dependent parameter α_i quantifies the symmetric broadening of the loss peak and consequently the broadening of the underlying distribution of relaxation times, relative to a Debye behavior (the latter corresponds to $\alpha = 1$ and exhibits a characteristic full width at half-maximum of 1.14 decades). The fits at 281, 305, and 325 K displayed in solid lines in Figure 3a are in good agreement with experimental data.

In an attempt to isolate the purely relaxational contribution from the conductivity contribution, the latter was systematically removed from the fitted curves. As shown in Figure 3b, this subtraction makes the two distinct secondary relaxation processes much more discernible. The data collected at "high temperature" (281−325 K) are reported in Figure 3b, whereas the "low-temperature" range (193−273 K) is displayed in Figure 3c. During each experiment, 22 different frequencies, ranging from 3×10^{-2} to 3×10^5 Hz, were scanned.

At high temperatures (Figure 3b), the observation of the β_1 peaks is hampered by the frequency limitation of the DEA 2970. The fact that the β_1 process could only be detected at low temperature (Figure 3c), with our dielectric device, suggests that this process is weakly activated. The existence of a second well-defined relaxation process of lower frequency, β_2, constitutes another outstanding feature of the dielectric spectra shown in Figure 3. With regard to the β_1 process, this second process occurs at lower frequencies and is characterized by dielectric peaks of smaller amplitude. This β_2 process shifts more rapidly toward low temperature, which indicates that it is more activated than β_1.

5.1. β_1 Relaxation Process. The β_1 relaxation process exhibits symmetrical loss peaks that are much broader than the 1.14 decades characteristic of a Debye process. As can be seen in Figure 3c, the peaks of the β_1 process become sharper when temperature increases (the width parameter $\alpha_{\beta_1}(T)$ varies from 0.29 at 193 K to 0.55 at 273 K). However, the width of the peaks remained important whatever the investigated temperature, which prevented us from deducing consistent information on $\Delta\epsilon_1(T) = (\epsilon_s - \epsilon_\infty)_1(T)$. The fit parameters τ_{β_1} and $\alpha_{\beta_1}(T)$ are reported in Table 1, for the temperature domain on which the β_1 process was fully observable.

The evolution of the relaxation times related to this secondary relaxation process β_1 is presented in the Arrhenius plot of Figure 4. We restricted the analysis to the temperature domain (193−290 K) where the β_1 peaks could be consistently fitted. The temperature dependence of the β_1 characteristic times exhibits an Arrhenius behavior over the explored temperature range. Extrapolation of this curve to the glass transition temperature

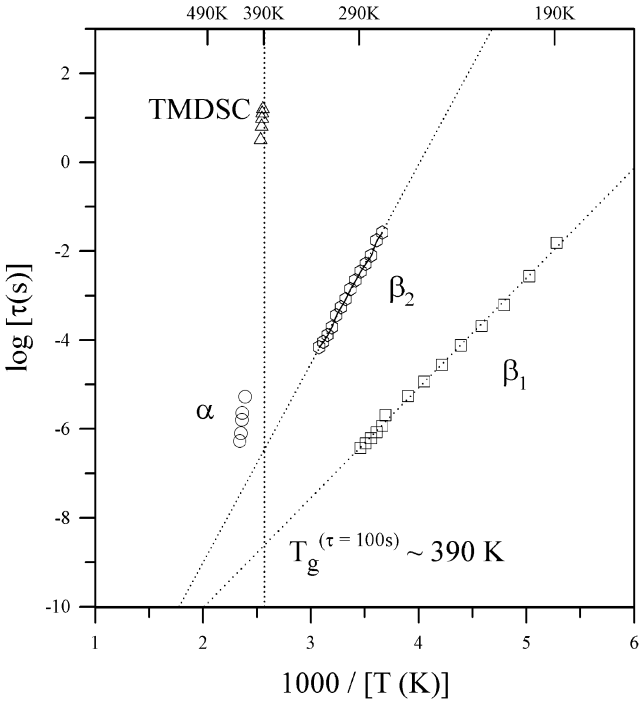

Figure 4. Arrhenius diagram for quenched trehalose, evidencing two distinct sub-T_g relaxation processes. Experimental data emanate from dielectric and specific heat spectroscopy measurements.

TABLE 1: Fit Parameters of the Cole−Cole Eq 12 for the Two Distinct β Processes Detected in Trehalose, over the Temperature Domains Where Their Respective $\epsilon''_\omega(T)$ Peaks Were Satisfyingly Discernible

β_1 process			β_2 process		
T, K	τ_{β_1}, s	α_{β_1}	T, K	τ_{β_2}, s	α_{b_2}
193	1.5×10^{-2}	0.29	277	1.7×10^{-2}	0.47
213	6.2×10^{-4}	0.36	289	3.5×10^{-3}	0.46
233	7.6×10^{-5}	0.41	301	8.4×10^{-4}	0.46
253	1.2×10^{-5}	0.49	313	1.8×10^{-4}	0.45
273	2.6×10^{-6}	0.55	325	6.9×10^{-5}	0.48

(at which $\tau = 100$ s) yields $\tau_{\beta_1}(T_g) = 2.36 \times 10^{-9}$ s. In an Arrhenius representation of the evolution of $\tau(T)$, the fit parameters for the β_1 process are $E_a = 47.2$ kJ/mol and $\tau = 10^{-15}$ s. Considering an Eyring phenomenological description of the relaxation, this latter result suggests that the activation entropy is almost 0.[36]

5.2. β_2 Relaxation Process. The dielectric peaks of the β_2 relaxation process are also symmetrical, but interestingly, no significant evolution of the width parameter $\alpha_{\beta_2}(T)$ could be observed over the temperature domain (277−325 K) where β_2 was detectable ($\alpha_{\beta_2} \approx 0.46$, see Table 1). It is also worth emphasising that the amplitude of the β_2 peaks remains fairly constant over the investigated temperature range. Similarly to that of the β_1 process, the temperature dependence of the characteristic times of the β_2 process exhibits an Arrhenius behavior over the explored temperature range. The fit parameters $\tau = 10^{-18}$ s and $E_a = 85.6$ kJ/mol imply a higher activation entropy than that of the β_1 process. One can also notice that the activation energy of the β_2 process is greater than that of the β_1 process, as can be seen from Figure 3.

6. Discussion

The combined use of two spectroscopic techniques, namely, TMDSC and dielectric analysis, allowed the detection of the relaxations in quenched anhydrous trehalose, above and below T_g. The following section is organized in two distinct parts. We first discuss the "above-T_g" results, with emphasis on the relation between fragility and nonexponentiality. A second paragraph is devoted to the "sub-T_g" results, and especially the origin of the secondary relaxations.

Specific heat spectroscopy was performed to investigate the mobility of supercooled trehalose above T_g. This analysis yielded a steepness index $m_{treh} = 107$, which attests to the very fragile character of trehalose. TMDSC data also provided an estimation of the stretching exponent of the KWW eq 11, $\beta_{KWW,treh} = 0.30$. It is worth emphasising that the β_{KWW} values determined by TMDSC come from measurements above T_g, in the equilibrium metastable liquid state. According to the correlation recognized by Böhmer et al.,[16] this very low value is consistent with the very fragile character of trehalose. However, such a small $\beta_{KWW,treh}$ does not fit accurately in the general trend highlighted by Böhmer, since this sugar appears to be less exponential in relaxation than expected. Specific heat spectroscopy has already been shown to be a powerful tool for the determination of m and β_{KWW}.[27] However, to make sure that our peculiar result on trehalose was not an artifact of the specific heat spectroscopy, we attempted to check whether this method was sensitive enough to measure very low stretching exponents. For this purpose, we evaluated the characteristics of polymethylmetacrylate (PMMA), a very fragile polymer of low stretching exponent ($m_{PMMA} = 145$ and $\beta_{KWW,PMMA} = 0.35$, as quoted in ref 16). We obtained for PMMA a stretching exponent of 0.30,[39] which is in good agreement with the value reported by Böhmer et al. in ref 16 and thus supports our analysis on trehalose. One may then wonder if the enhanced nonexponential behavior of trehalose, with regard to its fragility, is a common feature to all the disaccharides. Unfortunately, only few studies up to now dealt with the dynamical characteristics of pure disaccharides. Noel et al. investigated in 1996 the dielectric relaxation of anhydrous maltose, an isomer of trehalose.[37] The frequency domain they explored (10^3-10^5 Hz) is too far from the glass transition to allow a precise determination of m_{malt}. However, extrapolation of their Arrhenius diagram (Figure 6 from ref 37) to the T_g area indicates that m_{malt} should be higher than 75. Further analysis of Figure 7 from ref 36, which presents a normalized plot of the α relaxations for pure maltose, also shows that the stretching exponent for maltose is close to 0.32. Just like trehalose, maltose thus seems to be a fragile glass former with a lower stretching exponent than expected. Chan and co-workers studied the dielectric relaxations of the monosaccharide glucose,[38] which is the constituting unit of the trehalose molecule. They calculated the stretching exponent $\beta_{KWW,gluc} = 0.47$, and extrapolation of their characteristic times to T_g yielded $m_{gluc} \approx 75$. These results indicate that glucose conforms to the general pattern reported in ref 16. It follows from the above analyses that the stretching exponent β_{KWW} decreases with the molecular complexity. However, this decrease is more rapid than expected in the case of disaccharides. As a consequence, further investigations are needed to determine the possible origins of this apparent enhanced heterogeneity of the dynamics.

Another outstanding feature of the dynamic behavior of trehalose is the existence of two distinct sub-T_g relaxation processes, as revealed by the low-temperature dielectric spectra. The existence of such processes naturally raises the question of the origin of the sub-T_g relaxations, which is still a matter of controversy.[40] From this point of view, it is interesting to compare our results with those of other disaccharides.

Einfeldt and co-workers studied the sub-T_g relaxations of the monosaccharide glucose and four other polysaccharides con-

TABLE 2

	α at 213 K	E_a, kJ/mol
trehalose β_1 (2 GU)	0.36	47.2
cellobiose (2 GU)	0.50	32.8
gentiobiose (2 GU)	0.47	34.0
cellopentaose (5 GU)	0.32	51.5
cellulose (polymer)	0.34	43.5

stituted of glucose units: the disaccharides cellobiose and gentiobiose (two isomers of trehalose), the pentasaccharide cellopentaose, and the polymer cellulose.[41] They highlighted that the sub-T_g relaxation spectra of pure glucose differed strongly from those of the other compounds. Their investigations on glucose revealed a single near-Debye process ($\alpha^{gluc} = 0.94$), which occurs at distinctly smaller T/T_g and higher frequency than the β_1 process of trehalose. They attributed this type of relaxation to the reorientational motions of the side groups, with no evident discrimination between the hydroxyl and methylol groups. On the contrary, the other polysaccharides (cellobiose, cellopentaose, and cellulose) revealed much broader dielectric relaxation spectra, which display the signature of the so-called Johari-Goldstein process and occur at lower frequencies. On the basis of these dielectric studies, Einfeldt et al. suggested that such a distributed response was unlikely to reflect the motions of small side groups, such as OH or CH_2OH, and that this secondary relaxation process in polysaccharides should rather be attributed to local motions of chain segments. In pure trehalose, the dominant non-Debye sub-T_g process (β_1) differs clearly from the fast glucose process and can be assigned to the Johari-Goldstein relaxation observed in polysaccharides. As can be seen in Table 1, this β_1 process is characterized by a broad distribution of relaxation times, with α varying from 0.29 at 193 K to 0.55 at 273 K. Table 2 gathers together the values of the parameter α at 213 K and those of the activation energy of the β_1 process for trehalose and the four compounds investigated in ref 41. The number of glucose units (GU) that constitute the molecule is mentioned for each compound.

Table 2 clearly shows that, at 213 K, the temperature-dependent α parameter of trehalose is much smaller than those of its isomers cellobiose and gentiobiose. However, this difference is consistent with the fact that the glass transition temperature of trehalose is also higher (390 K versus 350 K for cellobiose). Therefore, if one transposes the comparison to the temperature "$T_g - 137$ K" (i.e., 213 K for cellobiose and 253 K for trehalose), α for trehalose is 0.49, which is similar to the values announced for the other disaccharides. However, if we now consider the activation energies listed above, the β_1 process in trehalose seems much closer to the secondary relaxations of large molecules (such as cellopentaose and the polymer cellulose) than to those of its isomers cellobiose and gentiobiose. Trehalose thus seems to display secondary relaxation features that would rather assimilate it with polysaccharides of higher molecular complexity. It is noteworthy that this trend is also discernible for the main relaxation: for the same molecular weight, trehalose shows a distinctly higher T_g value than the other disaccharides.

The β_2 process in trehalose appears as a shoulder on the low-frequency side of the β_1 peaks and also exhibits non-Debye behavior. It could only be observed over a narrow temperature domain, close to room temperature. It is worth pointing out that, again, this type of relaxation process has only been detected for more complex polysaccharides, like cellulose or dextran.[42] It has also been recently observed in maltitol.[43] However, the origin of such relaxation has not been clearly determined yet.

At last, it can be mentioned that other secondary relaxation processes are likely to be detected in glassy trehalose, in frequency regions made inaccessible to us by the dielectric analyzer limitations. Actually, dielectric studies on cellobiose[40] revealed the existence of a sub-T_g process, attributed to side-group rearrangements, that occurs at high frequencies (10^6 Hz at a temperature as low as $T_g - 200$ K), and it is reasonable to assume that glassy trehalose may exhibit the same kind of relaxation process.

In summary, this work has revealed several peculiar dynamic features of anhydrous supercooled trehalose, regarding both the main and secondary relaxation processes. The ability to form a glass and the intrinsic properties of this glassy state have been assumed to play a role in the bioprotection mechanism of trehalose,[15] which seems to be more efficient than that of the other disaccharides. This work shows that the characteristics of the sub-T_g mobility of trehalose are in accordance with those of polysaccharides of much higher molecular complexity. However, there are differences, and these differences cannot be attributed to the molecular weight but must originate from the nature of intermolecular bonds in trehalose,[20] which constitutes another point of interest with regard to biopreservation. One potential extension of this work is the investigation of possible unusual dynamic features of the trehalose/water solutions. This would allow us to get some insight on the behavior of trehalose in natural biopreservation conditions and to investigate the possible relations between dynamic properties and the "destructuring" effect[12] that has been evoked as a possible bioprotection mechanism.

Acknowledgment. We gratefully acknowledge the financial support from AVENTIS Pharma and Region Nord Pas de Calais. This work was performed in the frame of the ACI "Action bioprotectrice des sucres".

References and Notes

(1) Brown, G. M.; Rohrer, D. C.; Berking, B.; Beevers, C. A.; Gould, R. O.; Simpson, R. *Acta Crystallogr.* **1972**, *B28*, 3145.
(2) Taga, T.; Senma, M.; Osaki, K. *Acta Crystallogr.* **1972**, *B28*, 3258.
(3) Jeffrey, G. A.; Nanni, E. *Carbohydr. Res.* **1985**, *137*, 21.
(4) Reisener, H. J.; Goldschmid, H. R.; Ledingham, G. A.; Perlin, A. S. *Can. J. Biochem. Phys.* **1962**, *40*, 1248.
(5) Sussich, F.; Princivalle, F.; Cesaro, A. *J. Am. Chem. Soc.* **1998**, *120*, 7893.
(6) J. F. Willart De Gusseme, A.; Hemon, S.; Descamps, M.; Leveiller, F.; Rameau, A. *J. Phys. Chem. B* **2002**, *106*, 3365.
(7) Crowe, J. H.; Carpenter, J. F.; Crowe, L. M. *Annu. Rev. Physiol.* **1998**, *60*, 73.
(8) Crowe, L. M.; Mouradian, R.; Crowe, J. H.; Jackson, S. A.; Womersley, C. *Biochim. Biophys.* **1984**, *769*, 141.
(9) Branca, C.; Magazu, S.; Maisano, G.; Migliardo, P.; Tettamanti, E. *J. Mol. Struct.* **1999**, *480*−*481*, 133.
(10) Green, J. L.; Angell, C. A. *J. Phys. Chem.* **1989**, *93*, 2880.
(11) Roos, Y. H. In Phase Transitions in Foods; Academic Press: New York, 1995.
(12) Branca, C.; Magazu, S.; Maisano, G.; Migliardo, P.; Villari, V.; Sokolov, A. P. *J. Phys.: Condens. Matter* **1999**, *11*, 3823.
(13) Elias, M. E.; Elias, A. M. *J. Mol. Liq.* **1999**, *83*, 303.
(14) Ding, S.; Fan, J.; Green, J. L.; Lu, Q.; Angell, C. A. *J. Therm. Anal.* **1996**, *47*, 1391.
(15) Sussich, F.; Skopec, C.; Brady, J.; Cesaro, A. *Carbohydr. Res.* **2001**, *334*, 165. A corrigendum to this paper concerning the *m* values was published in: *Carbohydr. Res.* **2003**, *338*, 11, 1259.
(16) Böhmer, R.; Ngai, K. L.; Angell, C. A.; Plazek, D. J. *J. Chem. Phys.* **1993**, *99*, 5, 4201.
(17) Johari, G. P.; Goldstein, M. *J. Chem. Phys.* **1970**, *53*, 2372.
(18) Angell, C. A.; Ngai, K. L.; McKenna, G. B.; McMillan, P. F.; Martin, S. W. *J. Appl. Phys.* **2000**, *88*, 6, 3113.
(19) Hikima, T.; Hanaya, M.; Oguni, M. *Solid State Commun.* **1995**, *93*, 8, 713.
(20) Miller, D. P.; de Pablo, J. J.; Corti, H. *Pharm. Res.* **1997**, *14*, 5, 578.

(21) Plazek, D. J.; Ngai, K. L. *Macromolecules* **1991**, *24*, 1222.
(22) Shamblin, S. L.; Tang, X.; Chang, L.; Hancock, B. C.; Pikal, M. J. *J. Phys. Chem. B* **1999**, *103*, 4113.
(23) Hancock, B. C.; Shamblin, S. L. *Thermochim. Acta* **2001**, *380*, 95.
(24) Wunderlich, B.; Jim, Y.; Boller, A. *Thermochim. Acta* **1994**, *238*, 277.
(25) Bustin, O.; Descamps, M. *J. Chem. Phys.* **1999**, *110*, 22, 10982.
(26) Carpentier, L.; Bustin, O.; Descamps, M. *J. Phys. D: Appl. Phys* **2002**, *35*, 402.
(27) Carpentier, L.; Bourgeois, L.; Descamps, M. *J. Therm. Anal. Cal.* **2002**, *68*, 727.
(28) Jiang, Z.; Imrie, C. T.; Hutchinson, J. M. *Thermochim. Acta* **1998**, *315*, 1.
(29) Weyer, S.; Hensel, A.; Schick, C. *Thermochim. Acta* **1997**, *304*−*305*, 267.
(30) Ediger, M. D.; Angell, C. A.; Nagel, S. R. *J. Phys. Chem.* **1996**, *100*, 13200.
(31) Böhmer, R.; Angell, C. A. Local and Global Relaxations in glass forming materials. In *Disordered effects on relaxational processes*; Richert, R., Blumen, A., Eds.; Springer-Verlag: New York, 1994.
(32) Phillips, J. C. *Rep. Prog. Phys.* **1996**, *59*, 1133.
(33) Ngai, K. L.; Rendell, R. W.; Plazek, D. J. *J. Chem. Phys.* **1991**, *94*, 4, 3018.
(34) Böhmer, R.; Sanchez, E.; Angell, C. A. *J. Phys. Chem.* **1992**, *96*, 23, 9089.
(35) Moynihan, C. T.; Boesch, L. P.; Laberge, N. L.; *Phys. Chem. Glasses* **1973**, *14*, 6, 122.
(36) Kauzmann, W. *Rev. Mod. Phys.* **1942**, *1*, 12.
(37) Noel, T. R.; Parker, R.; Ring, S. G. *Carbohydr. Res.* **1996**, *282*, 193−206.
(38) Chan, R. K.; Pathmanathan, K.; Johari, G. P. *J. Phys. Chem.* **1986**, *90*, 6358.
(39) Carpentier, L.; Desprez, S.; Descamps, M., *unpublished results*.
(40) Ngai, K. L.; Lunkenheimer, P.; León, C.; Schneider, U.; Brand, R.; Loidl, A. *J. Chem. Phys.* **2001**, *1405*, 3.
(41) Meissner, D.; Einfeldt, J.; Kwasniewski, A. *J. Non-Cryst. Solids* **2000**, *275*, 199.
(42) Einfeldt, J.; Meissner, D.; Kwasniewski, A. *Prog. Polym. Sci.* **2001**, *26*, 1419.
(43) Carpentier, L.; Descamps, M. *J. Phys. Chem. B* **2002**, *107*, 271.